HHS Public Access

Author manuscript

J Phys Chem C Nanomater Interfaces. Author manuscript; available in PMC 2015 May 21.

Published in final edited form as:

J Phys Chem C Nanomater Interfaces. 2015 May 7; 119(18): 10048–10058. doi:10.1021/jp511448e.

Comparative Dynamics and Sequence Dependence of DNA and RNA Binding to Single Walled Carbon Nanotubes

Markita P. Landry[†], **Lela Vuković**[‡,§], **Sebastian Kruss**[†], **Gili Bisker**[†], **Alexandra M. Landry**[‖], **Shahrin Islam**[†], **Rishabh Jain**[†], **Klaus Schulten**[‡,§], and **Michael S. Strano**[*,†]

[†]Department of Chemical Engineering, Massachusetts Institute of Technology, 77 Massachusetts Avenue, Cambridge, Massachusetts 02139, United States

[‡]Department of Physics, University of Illinois at Urbana–Champaign, Champaign, Illinois 61820, United States

[§]Center for the Physics of Living Cells, University of Illinois at Urbana-Champaign, Champaign, Illinois 61820, United States

[‖]Department of Chemical Engineering, University of California at Berkeley, Berkeley, California 94720, United States

Abstract

Noncovalent polymer-single walled carbon nanotube (SWCNT) conjugates have gained recent interest due to their prevalent use as electrochemical and optical sensors, SWCNT-based therapeutics, and for SWCNT separation. However, little is known about the effects of polymer-SWCNT molecular interactions on functional properties of these conjugates. In this work, we show that SWCNT complexed with related polynucleotide polymers (DNA, RNA) have dramatically different fluorescence stability. Surprisingly, we find a difference of nearly 2500-fold in fluorescence emission between the most fluorescently stable DNA-SWCNT complex, C_{30} DNA-SWCNT, compared to the least fluorescently stable complex, $(AT)_7A$-$(GU)_7G$ DNA-RNA hybrid-SWCNT. We further reveal the existence of three regimes in which SWCNT fluorescence varies nonmonotonically with SWCNT concentration. We utilize molecular dynamics simulations to elucidate the conformation and atomic details of SWCNT-corona phase interactions. Our results show that variations in polynucleotide sequence or sugar backbone can lead to large changes in the conformational stability of the polymer SWCNT corona and the SWCNT optical response. Finally, we demonstrate the effect of the coronae on the response of a recently developed dopamine nanosensor, based on $(GT)_{15}$ DNA- and $(GU)_{15}$ RNA-SWCNT complexes. Our results clarify several features of the sequence dependence of corona phases produced by polynucleotides adsorbed to single walled carbon nanotubes, and the implications for molecular recognition in such phases.

[*]Corresponding Author: Phone: 617-324-4323. strano@mit.edu.

Introduction

Semiconducting single walled carbon nanotubes (SWCNT) are allotropes of carbon in the form of 1 nm diameter cylinders that hold a great promise for a variety of applications.[1] SWCNT have been used for the development of nanocomposite materials,[2] molecular detection agents,[3] molecular delivery vehicles,[4] electrochemical sensors,[5,6] optical sensors,[7–11] biologically compatible nanoconjugates,[12,13] and nanotube partitioning.[14–19] Many SWCNT applications rely on their noncovalent functionalization with physisorbed polymers, such that the sp2 hybridization of the honeycomb carbon lattice of the SWCNT surface remains intact and fluorescent. Adsorbed polymers create a molecular corona around the SWCNT, which can facilitate the incorporation of SWCNT into bulk materials,[20] make SWCNT water-soluble and biocompatible,[21] appropriate for targeted delivery into organelles,[7] or enable SWCNT-based sensing.[8,22] For the above reasons, much experimental and theoretical work has been done to understand noncovalent interactions that lead to well-dispersed aqueous SWCNT suspensions and their fluorescence.[23–26] In each of the above examples, most of which employ DNA or RNA polymers to form coronae, the structure of the polymer conjugated to the SWCNT is a crucial factor for the proper execution of the technology. Fundamental nucleotide-SWCNT interactions have enabled SWCNT length and chirality sorting,[18,27–29] SWCNT patterning and self- assembly,[30,31] and molecular detection.[8,22] Studies have shown that the substitution of a single functional unit of DNA, a nucleotide, can drastically alter its binding behavior on the SWCNT surface.[16,18,32] Consequently, there has been sustained interest in better understanding the behavior of DNA and RNA polymers in their interactions with SWCNT.

Of the many areas that hinge on noncovalent SWCNT encapsulation, understanding the structure and function of SWCNT coronae is particularly important for the development of optical sensors. However, it remains an ongoing research question to elucidate corona phase molecular interactions responsible for SWCNT colloidal stability and fluorescence modulation, which provide molecular recognition and the optical readout for SWCNT-based optical sensors. The SWCNT coating influences the local dielectric environment of the SWCNT[33] and, consequently, their fluorescence. Therefore, there is a strong interest in understanding the underlying contributions of the structure of the SWCNT corona to the stability and fluorescence of these SWCNT- corona constructs for sensing applications among others.

One of the most prevalent polymers used for SWCNT sensor corona phases are polynucleic acids. Recent work has shown that DNA- and RNA- wrapped SWCNT have yielded sensors for a variety of molecules.[34–40] Here, we compare two analogous polymer wrappings, $(GT)_{15}$ DNA and $(GU)_{15}$ RNA, both shown to act as optical sensors for dopamine.[9] We monitor the fluorescence of these polymer-SWCNT complexes as a readout of the polymer dynamics on the SWCNT, and support our experimental observations with all-atom molecular dynamics (MD) simulations. We demonstrate that both polymer chemistry and SWCNT concentration can have dramatic effects on the structure of the corona phase and the optical properties of the SWCNT suspension. As a proof of principle for the immediate utility of our findings, we show that optical sensor signals can be greatly enhanced at certain chemical corona phase and SWCNT concentration regimes. Our findings provide more

detailed insight on the noncovalent interactions of polymer-SWCNT suspensions, and lay the ground for future design of SWCNT-based technologies.

Experimental and Theoretical Methods

Materials

All chemicals were purchased from Sigma-Aldrich (U.S.A.) unless otherwise noted. Single-stranded DNA and RNA (ssDNA, ssRNA) and hybrid ssDNA-ssRNA sequences were purchased from IDT (USA). HiPco-SWCNT were purchased from Unidym and processed according to the suggestions by the manufacturer (extraction of non-SWCNT material by phase separation in water/hexane).

Preparation and Characterization of Wrapped SWCNTs. HiPCo SWCNT (Unidym) were encapsulated with nucleic acid polymers by dissolving the polymers in a 100 mM NaCl solution and adding 2:1 w/w ratio of HiPCo SWCNT. The mixture was sonicated for 30 min in a water bath. Subsequently, the mixture was sonicated with a direct probe-tip sonicator (Cole Parmer, 3 mm tip diameter) for 5 min at 40% amplitude in an ice bath. After sonication, the mixture was centrifuged at 16000g for 90 min to pellet and remove unsolubilized SWCNT clusters. The supernatant was purified with a Microcon YM-100 filter (Millipore, Billerica, MA, U.S.A.) to remove free DNA or RNA polymer from the solution, and to obtain dispersed DNA-SWCNT or RNA- SWCNT in phosphate buffered saline (PBS, pH = 7.4, 10 mM). All samples were analyzed by UV–vis–nIR spectrometer (Shimadzu UV-3101PC).

Time-Dependent Fluorescence Monitoring of Nucleic Acid SWCNT

Nucleic-acid wrapped SWCNTs were diluted in PBS to a concentration of 2 mg/L (absorption of 0.072 at 632 nm) from stock solutions of 100 mg/L, and immediately imaged postdilution in 200 μL aliquots. Dilutions and imaging were performed in individual wells of 96 well-plates (Microtest 96 Tissue Culture Plate, BD). The nIR fluorescence was collected on a Zeiss AxioVision inverted microscope that was coupled to a PI Acton SP2500 spectrometer and a Princeton Instruments InGaAs OMA V array detector. Each sample was excited by a 785 nm photodiode laser (450 mW) with an exposure time of 10 s. For experiments pertaining to the fluorescence response of SWCNT sensors to dopamine, 198 μL aliquots of $(GT)_{15}$-DNA or $(GU)_{15}$-RNA at 2 mg/L were imaged before and immediately after the addition of 2 μl dopamine to a final dopamine concentration of 100 μM.

Microfluidic Chamber Preparation for Single-Molecule Experiments

Microfluidic chambers for single-SWCNT fluorescence intensity conformation experiments were constructed as previously described.[9] Briefly, glass coverslips forming the microfluidic chambers were functionalized with (3-aminopropyl)triethoxysilane (APTES) in ethanol (1% APTES, 1% water), and rinsed thoroughly with water prior to sample perfusion. A total of 1 mg/L $(GT)_{15}$DNA- or $(GU)_{15}$RNA-SWCNT solution in PBS was introduced into the microfluidic channel and permitted to incubate for 1 h to allow for SWCNTs adsorption to the surface. Surfaces were subsequently rinsed with 100 μL PBS buffer to remove nonadhered sample before mounting the slide on the microscope stage.

Near-Infrared Fluorescence Microscopy

Single-SWCNT data were collected on an inverted total-internal reflection fluorescence (TIRF) microscope (Zeiss, Axiovert 200) equipped with a 100× objective (Zeiss, α-Plan-APOCHROMAT 100×/1.46 Oil DIC (UV) VIS-IR) attached to a 2D InGaAs CCD array (OMA-V 2D, Princeton Instruments). This TIRF microscope utilized a supercontinuum excitation source (NKT, SuperK Extreme EXR15). SWCNT fluorescence was excited by filtering the supercontinuum excitation light with a 632 nm band-pass filter (Semrock, FF02–632/22–25). The emission from the SWCNT was collected through a 980 nm long-pass filter (Semrock, BLP017–980R–25) prior to imaging with the InGaAs CCD array.

Molecular Dynamics Simulations

Interactions of SWCNT coated with ssDNA and ssRNA polymers were examined in all-atom MD simulations. (8,8) SWCNTs of length l = 73 Å, built with VMD plugin Carbon Nanostructure Builder,[41] were used in all the simulations. $(GT)_{15}$DNA, $(C)_{30}$DNA, $(GU)_{15}$RNA, and $(AC)_{15}$RNA strands were prepared with 3DNA software[42] in conformations observed in canonical duplexes. The strands were placed ≈15 Å away from the SWCNT, with their long axes parallel to the SWCNT axes. Na^+ counterions, which neutralized nucleic acid charges, were placed with a VMD plugin cionize at potential energy minima of prepared SWCNT-nucleic acid systems. The neutralized systems were solvated in TIP3P water and 50 mM NaCl, with solvate and ionize VMD plugins, respectively.[41] The completed systems contained approximately 77000 atoms.

MD simulations were performed with NAMD2.9 software.[43] The systems were described with the CHARMM27 force field,[44] with SWCNT atoms described as benzene-type atoms (CA). To verify that the observed phenomena is force field independent, one simulation of SWCNT coated with $(GU)_7$-RNA was performed with the AMBER force field with SB[45] and BSC0[46] corrections. In all simulations, the particle-mesh Ewald (PME) method[47] was used for evaluation of long-range Coulomb interactions. The time step was set to 2.0 fs, and long-range interactions were evaluated every 1 (van der Waals) and 2 time steps (Coulombic). After 2000 steps of minimization, ions and water molecules were equilibrated for 2 ns around the SWCNTs and nucleic acids, which were restrained using harmonic forces with a spring constant of 1 kcal/mol$Å^2$. Then, systems were simulated for 250 ns with nucleic acid strands unrestrained, while the SWCNT remained restrained. The simulations were performed in the NpT ensemble, at a constant temperature T = 310 K, a Langevin constant γ_{Lang} = 1.0 ps^{-1}, and at a constant pressure p = 1 bar.

Results and Discussion

DNA Shows Increased Conformational Stability on SWCNT over RNA

To probe the conformational stability of RNA and DNA polymers on SWCNT, we conducted a series of experiments following the seminal work of Coleman et al.[48] Previous studies have shown that the gradual wrapping of SWCNT with dsDNA can be monitored using an increase in the SWCNT nIR fluorescence.[48] A 275 min time-lapse assay of the fluorescence spectra of multichiral $(GT)_{15}$ DNA-SWCNT and $(GU)_{15}$ RNA-SWCNT samples after dilution to 2 mg/L in PBS, shown in Figure 1a,b, have a gradual increase in

fluorescence, which is more pronounced for smaller SWCNT diameters. We attribute this increase in fluorescence to a gradual stacking of the nucleotide polymer bases on the SWCNT surface. The increase in fluorescence is more prevalent for $(GU)_{15}$ RNA, suggesting that the DNA-SWCNT corona phase is more conformationally robust on the SWCNT surface than RNA-SWCNT coronas. We propose that nucleotide polymer equilibration via base-SWCNT stacking causes water exclusion from the SWCNT surface. As water is a known quencher of SWCNT fluorescence, its substitution by nucleotide bases creates an increase in SWCNT photoemission.[49] Therefore, the change in SWCNT fluorescence is a measure of an initially imperfect polynucleotide wrapping gradually undergoing stabilization on the SWCNT surface. It is unlikely that this increase in fluorescence is due to SWCNT aggregation, as only individually encapsulated SWCNT undergo fluorescence emission.[50]

Figure 1c shows the time-dependent relative changes in SWCNT fluorescence for all SWCNT chiralities wrapped with $(GT)_{15}$ DNA (blue) and all SWCNT chiralities wrapped with $(GU)_{15}$ RNA (red). Fluorescence readings are obtained by extracting peak intensities in the spectra shown in Figures 1a-b, where each peak corresponds to a distinct SWCNT chirality.

The results in Figure 1c show that, for all SWCNT chiralities, $(GU)_{15}$ RNA undergoes significantly more rearrangement on the SWCNT than (GT)15 DNA over the course of 275 min. Circular dichroism experiments for $(GU)_{15}$ RNA-SWCNT and $(GT)_{15}$ DNA-SWCNT suspensions from which free DNA or RNA polymers have been filtered out show no change in the CD spectra over the course of an hour. As previous studies have shown, an invariant CD spectra suggests no net polymer desorption from the SWCNT.[51] Furthermore, as our DNA- and RNA-SWCNT suspensions have free nucleic acid polymers removed from solution, the ongoing stability of our DNA- and RNA-SWCNT suspension strongly suggests that both DNA and RNA polymers remain adsorbed to the SWCNT surface. Therefore, we attribute the change in fluorescence to polymer rearrangement and not polymer desorption or SWCNT aggregation.[48]

The increase in SWCNT intensity after dilution from 100 to 1 mg/L in PBS buffer is initially rapid, and slows down as the DNA or RNA polymer equilibrates on the SWCNT surface within 275 min (Figure 1c). We hypothesize that the gradual rearrangement of the polymer, and the subsequent stacking of individual nucleotide bases along the surface of the SWCNT leads to this time-dependent fluorescence increase. Therefore, we model the systems using a base-stacking kinetic model. This model, used to fit our data for $(GT)_{15}$ DNA–SWCNT and $(GU)_{15}$ RNA–SWCNT, for SWCNTs of (7,5) chirality, shows that bases stack with negative cooperativity among individual nucleotides. Furthermore, the model shows that stiffness of RNA, which is larger than stiffness of DNA, contributes to the more drastic rearrangement of RNA polynucleotides on the SWCNT surface.

To further investigate the contribution of the polymer properties to the SWCNT corona phase conformation, we expanded our polymer library and repeated our analysis of SWCNT fluorescence modulation. Figure 2 shows the fluorescence change for the emission peak at 1133 nm (corresponding to the (9,4) chirality SWCNT33), extracted from spectra of

solutions with multichiral SWCNT wrapped with DNA, RNA, and DNA–RNA polymer hybrids of varying lengths and sequences. Traces are color coded to represent DNA sequences (red), RNA sequences (black), and DNA– RNA hybrid sequences (green). Responses are recorded for the (9,4) chirality SWCNT at ∼1133 nm, for the same 275 min experimental time frame as data shown in Figure 1. The results in Figure 2 show that, generally, DNA has much greater conformational stability on SWCNT than RNA or DNA–RNA polymer hybrids. The most conformationally stable DNA-SWCNT complex, C_{30} DNA-SWCNT, undergoes nearly 2500-fold less fluorescence modulation than the least conformationally stable complex, AT_7A-GU_7G RNA-DNA hydbrid-SWCNT. A notable exception is the case of the $G_{15}T_{15}$ DNA-SWCNT complex, which shows a 6-fold change in fluorescence within the 275 min experiment. We attribute this exception to the formation of G-quadruplex structures in the 15-repeat guanine DNA sequence.[52] As an additional control, we verified that nonirradiated RNA-SWCNT samples also exhibit similar fluorescence increase as did irradiated samples, to ensure that laser irradiation was not the cause of the change in RNA-SWCNT fluorescence.

SWCNT Fluorescence Varies Non-Monotonically with SWCNT Concentration

Fluorescence increases due to polymer nucleotide stacking on SWCNT, as observed in equilibration experiments (Figure 1), are likely contributing to the fluorescence signal of our SWCNT samples. Nucleotides that stack strongly on the SWCNT surface increase SWCNT fluorescence by shielding the SWCNT from water molecules that quench fluorescence. As such, we expect SWCNT fluorescence to be (1) directly proportional to the ability of DNA or RNA nucleotides to stack on the SWCNT surface, and (2) inversely proportional to the degree of water-induced quenching on the SWCNT surface for loosely stacked nucleotides.

The effect of SWCNT concentration on the 1133 nm fluorescence of the (9,4) chirality SWCNT was examined for serial dilutions of $(GT)_{15}$ DNA-SWCNT and $(GU)_{15}$ RNA-SWCNT samples. Fluorescence readings were recorded 24 h after dilution from a stock solution of 100 mg/L SWCNT, to ensure the measurements were taken at equilibrium. The fluorescence intensity of both samples increases with SWCNT concentration in the SWCNT concentration range of 1 mg/L through 10 mg/L (Figure 3a), which is likely due to the increase in the concentration of SWCNT, the emitter. Little fluorescence is observed for both samples in the concentration range 10^{-2}–0.1 mg/L SWCNT, where there are fewer SWCNT emitters. However, at 10^{-2} mg/L SWCNT and below, SWCNT fluorescence is recovered drastically and increases nonlinearly with decreasing SWCNT concentration (Figure 3a).

A quick calculation using an average polynucleotide-SWCNT diameter of 3 nm, and average SWCNT length of 300 nm, estimating the average distance between molecules as $V^{1/3}$ per molecule suggests that, for “high” SWCNT concentrations above 1 mg/L, individual SWCNT complexes are approximately a few hundred nanometers apart on average, for “intermediate” SWCNT concentrations from 0.1–10^{-2} mg/L, individual SWCNT complexes are about one micron apart on average, and for “low” SWCNT concentrations below 10^{-2} mg/L SWCNT, individual SWCNT complexes are several tens of microns apart on average. Therefore, at “high” SWCNT concentrations, inter-SWCNT

distances are on the order of the length of a single SWCNT complex, and neighboring SWCNT are therefore likely to interact frequently, whereas at “low” SWCNT concentrations, individual complexes are several microns apart, making physical or electrostatic interactions infrequent.

The sudden and drastic recovery in SWCNT fluorescence at low SWCNT concentrations occurs when the sample concentration is low enough such that individual polynucleotide–SWCNT complexes are not influenced by neighboring complexes, either electrostatically or due to interactions of polynucleotides adsorbing between multiple neighboring SWCNT (Figure 3a, green). When SWCNT concentrations are in the range of 10^{-2}–0.1 mg/L, electrostatic or physical interactions between corona phases of neighboring SWCNT become increasingly prevalent. These interactions could cause partial dissociation of neighboring tightly bound nucleotides or binding of polynucleotide polymers to multiple adjacent SWCNT, creating a DNA or RNA corona in which nucleotides and water interchangeably stack to the SWCNT surface. As water molecules penetrate the SWCNT corona interchangeably due to more loosely stacked nucleotides or stacking of neighboring polynucleotides, SWCNT fluorescence is quenched. Above 10^{0} mg/L, neighboring interactions become sufficiently prevalent to enable interbinding of nucleotides from neighboring polynucleotide-SWCNT complexes. Furthermore, the sheer number of bases stacking to the SWCNT to occlude surface water enables the recovery of fluorescence in this SWCNT concentration range (Figure 3a, purple). We note that the effects of nucleotide stacking and water occlusion within the SWCNT corona increase the fluorescence of the polynucleotide-SWCNT solution by a surprising magnitude: despite a 1000-fold drop in SWCNT concentration, a 2-fold increase in $(GT)_{15}$ DNA-SWCNT fluorescence, and a 2.5-fold increase in $(GU)_{15}$ RNA-SWCNT fluorescence is observed.

Our results show a surprising nonmonotonic dependence of SWCNT fluorescence on SWCNT concentration, where the highest net fluorescence is observed in the low SWCNT concentration regime. We hypothesize that high fluorescence at low SWCNT concentrations is due to tight stacking of nucleotide bases on SWCNT that occlude quenching water. In addition, we hypothesize that the transition from tightly to loosely-stacked nucleotides occurs due to electrostatic interactions between polymers from neighboring SWCNT complexes that increases with SWCNT concentration. These hypotheses were examined in a concentration dependent model, which explores the relationship between the concentration, the phase of the DNA or RNA on the SWCNT corona, and the resulting intensity of the sample. The resulting model fits of concentration dependent fluorescence responses of DNA and RNA polynucleotides, plotted in Figure 3a as grey dotted lines, are in good agreement with experimental data.

Single-Molecule Studies of Surface-Adhered Polynucleotide-SWCNT Show Stable Fluorescence

To eliminate the effects of SWCNT interparticle interactions and polymer rearrangement from sample fluorescence measurements, we studied $(GT)_{15}$ DNA- SWCNT and $(GU)_{15}$ RNA-SWCNT on the single molecule scale. To do so, both samples were surface-immobilized on a microfluidic imaging surface, such that the sample concentration enabled

visualization of individual SWCNT. We removed unbound polymer-SWCNT from the sample by flushing our microfluidic channel with three volumes of 100 μL PBS buffer prior to imaging, to ensure there were no interactions between individually dispersed SWCNT. We used a near-infrared total-internal reflection fluorescence (TIRF) microscope with 658 nm excitation to monitor the near-infrared emission intensity of individual surface-adhered polynucleotide-SWCNT for over 30 min (Figure 4a).

Throughout the course of the imaging, we observed no significant intensity fluctuations from individual SWCNT from either sample, as shown in the representative intensity-time traces from each sample (Figure 4b). Moreover, the normalized intensity changes for individual polynucleotide-SWCNT from each surface-immobilized sample were negligible at (I-Io)/Io = 0.01 ± 0.03 for $(GT)_{15}$ DNA-SWCNT and 0.03 ± 0.05 for $(GU)_{15}$ RNA-SWCNT (mean ± standard error). In contrast, the normalized intensity changes for solution-phase samples were at (I − Io)/Io = 0.24 ± 0.17 for $(GT)_{15}$ DNA-SWCNT and 1.74 ± 0.26 for $(GU)_{15}$ RNA-SWCNT (mean ± standard error). These results suggest that solution-phase interactions between polynucleotide wrappings of neighboring complexes, and polynucleotide stacking dynamics, contribute in large part to the time-dependent fluorescence modulation observed in Figure 1, and the concentration-dependent fluorescence modulation observed in Figure 3. Both interpolynucleotide corona interactions and intrapolynucleotide rearrangements are absent in our single-molecule studies, leading to the SWCNT fluorescence stability observed in Figure 4.

As a control, we also performed transmission electron microscopy (TEM) imaging of our $(GT)_{15}$ DNA-SWCNT and $(GU)_{15}$ RNA-SWCNT samples to probe the structure and dispersion of each sample. We specifically selected a concentration in the “high SWCNT concentration” regime (Figure 3, purple), to capture the probable interactions between neighboring polynucleotide-SWCNT complexes. A total of 10 mg/L of each sample was deposited onto a carbon film substrate and imaged. Mostly singly dispersed $(GT)_{15}$ DNA-SWCNT were observed, with a few occasional interparticle interactions. On the contrary, for the same concentration of $(GU)_{15}$ RNA-SWCNT, the sample showed a tendency to form parallel associations between multiple $(GU)_{15}$ RNA-SWCNT molecules. We note that TEM images were acquired in the solid phase, after polynucleotide-SWCNT drying, and may not fully represent the liquid-phase state of each sample. However, the differences between $(GT)_{15}$ DNA and $(GU)_{15}$ RNA TEM images suggest that the energy barrier for $(GT)_{15}$ DNA stacking on SWCNT is lower than for $(GU)_{15}$ RNA, leading to singly dispersed DNA samples and parallel bundling of RNA samples.

Concentration-Dependent SWCNT Fluorescence Contributes to Sensor Response

Recent developments in the field of nanosensors have provided researchers with useful tools for detection of important molecules. Many approaches to molecular detection rely on noncovalent conjugation of polymers around a semiconducting single-wall carbon nanotube to form a “corona” capable of molecular recognition. A recent development in corona-phase molecular recognition-based sensors has produced a sensor for neurotransmitters such as dopamine. Both $(GT)_{15}$ DNA-SWCNT and $(GU)_{15}$ RNA- SWCNT are optical sensors for dopamine, showing a strong turn-on response upon exposure to dopamine.[9] Given the large

variation in sample intensities as a function of SWCNT concentration, we explored whether sensor response could be optimized by simply varying SWCNT sensor concentration.

We tested the absolute DNA- or RNA-SWCNT response to dopamine, $(I - I_0)/I_0$, for (9,4) chirality SWCNT at ~1133 nm as a function of SWCNT concentration. As expected for a response normalized to the initial SWCNT intensity, $(GT)_{15}$ DNA-SWCNT does not show a significant SWCNT concentration-dependent response to dopamine above 1 mg/L SWCNT (Figure 3b). Interestingly, we observe a strong SWCNT concentration-dependent sensor response to dopamine for $(GU)_{15}$ RNA above 1 mg/L SWCNT (Figure 3c). For both $(GU)_{15}$ RNA-SWCNT and $(GT)_{15}$ DNA-SWCNT, sensor samples at concentrations below 10^{-2} mg/L regain a strong sensor response to dopamine (Figure 3b and c). These concentration-dependent effects mirror the initial fluorescence dependence on SWCNT concentration (Figure 3a). We show that a sensor's optical response can vary greatly depending on the nucleotide stacking conformation of the polymer on the SWCNT surface. This proof-of-principle experiment suggests that the interaction of the dopamine analyte with the SWCNT polynucleotide corona can easily be optimized to maximize sensor response by simply choosing an optimal working concentration.

DNA Binds More Strongly to SWCNT than RNA according to MD Simulations

Our experiments to date suggest that nucleotide stacking plays a dominant role in the time-dependent SWCNT fluorescence modulation we observe in Figure 1, and the concentration-dependent SWCNT fluorescence modulation we observe in Figure 2. We also consistently observe greater fluorescence modulation for $(GU)_{15}$ RNA-SWCNT over $(GT)_{15}$ DNA-SWCNT. To study these effects in greater detail and elucidate the atomic details of our polynucleotide-SWCNT samples, we performed a series of MD simulations. Molecular dynamics is a powerful tool to study the structure of SWCNT wrapped with ssDNA[53–55] and ssRNA.[56] To further probe molecular interactions leading to the conformation of SWCNT corona phases, we undertook a series of supporting molecular dynamics simulations of $(GT)_{15}$ DNA-SWCNT, $(GU)_{15}$ RNA-SWCNT, and $(AC)_{15}$ RNA- SWCNT in aqueous salt solutions. While nucleic acid polymers and SWCNT were initially not in contact in simulation boxes, nucleic acids quickly approached and started binding to SWCNTs during equilibration (within 10 ns). Eventually, nucleotide bases stacked on the SWCNT surfaces via the nucleotide aromatic rings, with nucleotide phosphate backbones pointing into the aqueous solution.

Differences in DNA-SWCNT and RNA-SWCNT binding modes can be seen in Figure 5a. After 250 ns, most DNA nucleotides stacked on the SWCNT, and the DNA strand laid largely flat while diffusing on the SWCNT surface. On the other hand, the RNA strand showed more self-interaction via off-SWCNT secondary structure formation, and therefore had fewer nucleotides bound to the SWCNT. RNA bases had a larger tendency to stack on each other than DNA bases, thus forming clusters solvated in the solution above the SWCNT surface (observed clusters circled in Figure 5a; ssRNA formed larger clusters than ssDNA). We simulated $(C)_{30}$ DNA- SWCNT as well, as it is the only nucleotide corona that showed no increase in fluorescence over the course of 275 min (Figure 2). To quantify differences between DNA and RNA stacking on the SWCNT surface, we evaluated radial

distribution of nucleic acid phosphate groups with respect to the central axis of SWCNT. Figure 5b shows that ssDNA stays mostly within 15 Å of the SWCNT surface, while ssRNA has a broader distribution and extends up to ∼22 Å away from the SWCNT surface. Two RNA strands show similar broad distribution profiles (broader than DNA), indicating that nucleotide binding modes have a strong dependence on the nature of the polynucleotide backbone (DNA or RNA). These effects can be further modulated by polynucleotide sequence. In contrast, the $(C)_{30}$ DNA-SWCNT distribution profile peaks sharply and is the only sequence that does not extend outside of 14 Å. To further quantify the binding of nucleic acid strands to SWCNTs, we plot SWCNT-nucleic acid contact areas in Figure 5c, which clearly shows that fewer RNA bases than DNA bases stack onto SWCNTs. Contact areas between SWCNT and $(GU)_{15}$ RNA and $(AC)_{15}$ RNA is 30% and 20% smaller than for $(GT)_{15}$ DNA, respectively. Since DNA covers a larger area of the nanotube, it also has larger interaction energies with the SWCNT than either of the RNA strands, as shown in Figure 5d. Interaction energies of single nucleotides with SWCNTs are of similar magnitude, as shown in Table S1. The observations reported in Figure 5 have also been reproduced in independent duplicate simulations of SWCNT with each of the $(GT)_{15}$ DNA, $(GU)_{15}$ RNA and $(AC)_{15}$ RNA strands. Therefore, it follows that properties of nucleotides linked into a polymer (e.g., polymer rigidity) contribute to the difference in base stacking abilities of ssDNA and ssRNA, in addition to the increased tendency of RNA to form off-SWCNT secondary structures that work against nucleotide-SWCNT stacking.

An interesting observation can be made from tracking dynamics of equilibrated strands bound to SWCNT in solution. Since most DNA nucleotides are bound to SWCNT, they diffuse quickly lateral to the SWCNT surface. In contrast, RNA strands appear more rigid, and the RNA nucleotide motion appears correlated in their lateral diffusion. In addition, RNA forms clusters of several nucleotides stacked on each other, which diffuse more slowly than free nucleotides along the SWCNT surface. Due to differences in binding, the DNA strand appears to be more flexible as its nucleotides act independently, while the RNA strand appears more rigid. Similar experimental observations were reported recently for ssRNA in solution; ssRNA was found to have shorter contour length, longer persistence length and higher rigidity than ssDNA.[34]

Sugar Conformations of RNA Nucleotides Shift Upon Binding to SWCNTs

The main chemical difference between DNA and RNA nucleotides is the presence of 2′-OH groups on RNA sugar rings. This chemical difference leads to differences in structural forms of DNA and RNA polymer strands. Typically, RNA sugar rings assume the so-called C3′-endo conformation, while DNA sugar rings assume the C2′-endo conformation, shown in Figure 6a. To understand why fewer RNA nucleotides than DNA nucleotides bind to SWCNTs, we closely examine the behavior of 2′-OH group and sugar conformations of these nucleotides in simulated trajectories.

Sugar rings of stacked DNA nucleotides can assume two orientations, where either the O4′ atom or one of the nonpolar carbon atom groups of the sugar ring come in contact with the SWCNT surface. RNA nucleotides stacking on SWCNT have either O4′ or O2′ atoms of the sugar ring in contact with the SWCNT surface, as shown in Figure 6b. The microscopic

picture that emerges from simulations is that sugar rings of RNA nucleotides whose 2′ OH groups point toward the SWCNT surface have predominant C3′-endo conformation, with occasional switches to C2′-endo conformation. On the other hand, it is the RNA sugar rings whose O4′ oxygen atoms point toward the SWCNT surface that switches to C2′-endo conformation upon stacking to the SWCNT (Figure 6b). Once ssRNA nucleotides stack with their O4′ atoms pointing to SWCNT surface and switch to C2′-endo conformation, their 2′-OH groups can hydrogen bond to a neighboring phosphate group (also seen in Figure 6b); it is this bond that likely contributes to stabilization of C2′-endo conformation.

We investigated whether the population of RNA nucleotides in the C2′-endo conformation, when stacked to a SWCNT surface, represents a significant conformational shift compared to unstacked bases. In Figure 6c, we plot distributions from complete MD simulations of dihedral angle γ, defined in Figure 6a as the relative position of C2′ and C3′ carbons, which characterizes the sugar conformation of a nucleotide. The plot shows separate γ values for SWCNT-stacked nucleotides and nucleotides that are not stacked (but are pointing into solution or stacking on nearby nucleotides). The plot confirms that all DNA nucleotides have a strong preference for the C2′-endo conformation, as expected, irrespective of stacking to SWCNT. RNA nucleotides that are not stacked onto SWCNT mostly assume the expected C3′-endo conformation. However, a significant fraction of RNA nucleotides (≈50%) shifts to C2′- endo conformation upon binding to SWCNTs. The effect that RNA sugar conformations shift to C2′-endo conformations upon binding to SWCNTs was confirmed to be independent of sequence and the force field; the effect was observed for $(AC)_{15}$ RNA-SWCNT complexes described with the CHARMM force field and $(GU)_7$ RNA-SWCNT complexes described with the AMBER force field. These molecular details could explain why DNA nucleotides stack more readily and less reversibly to SWCNT than RNA nucleotides. Our experimental observations consistently show greater time- and concentration-dependent fluorescence variability for RNA samples over DNA samples (Figures 1–3), results which can also be clarified with these MD results.

The performed simulations indicate two potential factors that could contribute to lesser conformational stability of ssRNA on SWCNT in comparison to ssDNA, as indicated in Figure 5a,c,d. In order to bind to SWCNT, both ssRNA and ssDNA need to overcome the barrier of separating neighboring nucleotides that stack on each other in solution. The first factor is that ssRNA has an additional barrier to overcome in comparison to ssDNA: stacked nucleotides of ssRNA in solution are stabilized by the 2′-OH group forming hydrogen bonds with either O4′ atom of a neighboring nucleotide or a phosphate group bridging the two neighboring nucleotides. Once that 2′-OH hydrogen bond is broken, a significant fraction of RNA nucleotides needs to also overcome the barrier of switching the value of the dihedral γ (C3′-endo → C2′-endo; the transition was found to be unfavorable by ∼6 kcal/mol for short RNA duplexes[33]). The second factor is that when ssRNA stacks onto SWCNT, its sugar ring almost always has polar oxygen atoms pointing toward the SWCNT surface (Figure 6b). On the other hand, ssDNA nucleotides can stack on SWCNT so that nonpolar carbon atoms of their sugar rings point to the SWCNT surface. Polar oxygen atoms of RNA are likely to prefer solvated state, which may lead to further destabilization of ssRNA stacking on SWCNT. We point out that the larger overall energy barrier for RNA base stacking to SWCNT over DNA base leads to a more dynamic environment in which water occlusion

from the SWCNT surface occurs more dynamically for RNA-based SWCNT samples. This is in line with our experimental observations that RNA-suspended SWCNT show greater time-dependent fluorescence variability than DNA-based SWCNT samples (Figure 2).

Here, we would like to note that the observed higher rigidity of ssRNA in comparison to ssDNA is likely due to additional hydrogen bonds between 2′-OH groups and neighboring nucleotides of RNA, shown in Figures 6b and S8b, which are missing from ssDNA. Stronger bonds between neighboring nucleotides lead to increased correlation in dynamics of these neighboring RNA nucleotides.

Conclusion

Our results show that very slight variations in the chemical structure of a polymer forming a SWCNT corona can have drastic effects on the fluorescence of SWCNT. We've shown that $(GU)_{15}$ RNA adopts a lower conformational stability on SWCNT than its $(GT)_{15}$ DNA counterpart, leading to solution phase changes in SWCNT fluorescence that can increase by over an order of magnitude. Molecular dynamics simulation results suggest that molecular interactions between polynucleotide polymers and SWCNT surfaces result in changes to polymer conformational stability, and lead to the observed fluorescence changes. Lastly, we show how the fluorescence responses of $(GT)_{15}$ DNA-SWCNT and $(GU)_{15}$ RNA-SWCNT sensors can vary drastically due to the differences in polymer-SWCNT conformation. Our results are relevant for a variety of fields in nanomaterials, sensor development, and fields with an inherent interest in developing methods for SWCNT brightening.[57]

Supplementary Material

Refer to Web version on PubMed Central for supplementary material.

Acknowledgments

We thank Dong Soo Yun for assistance with TEM imaging and members of the Strano and Schulten group for useful discussions. We gratefully acknowledge computer time provided by the Texas Advanced Computing Center (XSEDE allocation MCA93S028 to K.S.) and by the Computational Science and Engineering Program at the University of Illinois (Taub computing cluster). This work was supported by the National Science Foundation (Grant NSF-PHY-0822613 and NSF-PHY1430124, K.S.) and National Institutes of Health (grant NIH 9P41GM104601, K.S.). S.K. was supported by a postdoc fellowship from Deutsche Forschungsgemeinschaft (DFG). M.P.L. acknowledges an NSF postdoctoral research fellowship under Award No. 1306229, and a Burroughs Wellcome Fund grant under Award No. 1013994. M.S.S acknowledges partial support of this work by the National Science Foundation under award number 1213622. This work was partially supported by Cancer Center Support (core) Grant P30-CA14051 from the NCI. L.V. acknowledges support as an NSF Center for the Physics of Living Cells (CPLC) Postdoctoral Fellow.

References

1. Wang C, Takei K, Takahashi T, Javey A. Carbon Nanotube Electronics–Moving Forward. Chem Soc Rev. 2013; 42:2592–2609. [PubMed: 23229523]
2. Marconnet AM, Yamamoto N, Panzer MA, Wardle BL, Goodson KE. Thermal Conduction in Aligned Carbon Nanotube- Polymer Nanocomposites with High Packing Density. ACS Nano. 2011; 5:4818–4825. [PubMed: 21598962]
3. Pengfei QF, Vermesh O, Grecu M, Javey A, Wang O, Dai HJ, Peng S, Cho KJ. Toward Large Arrays of Multiplex Functionalized Carbon Nanotube Sensors for Highly Sensitive and Selective Molecular Detection. Nano Lett. 2003; 3:347–351.

4. Bates K, Kostarelos K. Carbon Nanotubes as Vectors for Gene Therapy: Past Achievements, Present Challenges and Future Goals. Adv Drug Delivery Rev. 2013; 65:2023–2033.
5. Jacobs CB, Peairs MJ, Venton BJ. Review: Carbon Nanotube Based Electrochemical Sensors for Biomolecules. Anal Chim Acta. 2010; 662:105–127. [PubMed: 20171310]
6. Sha J, Hasan T, Milana S, Bertulli C, Bell NAW, Privitera G, Ni Z, Chen Y, Bonaccorso F, Ferrari AC, et al. Nanotubes Complexed with DNA and Proteins for Resistive-Pulse Sensing. ACS Nano. 2013; 7:8857–8869. [PubMed: 24066614]
7. Giraldo JP, Landry MP, Faltermeier SM, McNicholas TP, Iverson NM, Boghossian AA, Reuel NF, Hilmer AJ, Sen F, Brew JA, et al. Plant Nanobionics Approach to Augment Photosynthesis and Biochemical Sensing. Nat Mater. 2014; 13:400–408. [PubMed: 24633343]
8. Zhang J, Landry MP, Barone PW, Kim J, Lin S, Ulissi ZW, Lin D, Mu B, Boghossian AA, Hilmer AJ, et al. Molecular Recognition Using Corona Phase Complexes Made of Synthetic Polymers Adsorbed on Carbon Nanotubes. Nat Nanotechnol. 2013; 8:959–968. [PubMed: 24270641]
9. Kruss S, Landry MP, Vander Ende E, Lima BMA, Reuel NF, Zhang JQ, Nelson J, Mu B, Hilmer A, Strano MS. Neurotransmitter Detection Using Corona Phase Molecular Recog- nition on Fluorescent Single-Walled Carbon Nanotube Sensors. J Am Chem Soc. 2014; 136:713–724. [PubMed: 24354436]
10. Landry MP, Kruss S, Nelson JT, Bisker G, Iverson NM, Reuel NF, Strano MS. Experimental Tools to Study Molecular Recognition within the Nanoparticle Corona. Sensors (Basel). 2014; 14:16196–16211. [PubMed: 25184487]
11. Kruss S, Hilmer AJ, Zhang JQ, Reuel NF, Mu B, Strano MS. Carbon Nanotubes as Optical Biomedical Sensors. Adv Drug Delivery Rev. 2013; 65:1933–1950.
12. Sapsford KE, Algar WR, Berti L, Gemmill KB, Casey BJ, Oh E, Stewart MH, Medintz IL. Functionalizing Nanoparticles with Biological Molecules: Developing Chemistries That Facilitate Nanotechnology. Chem Rev. 2013; 113:1904–2074. [PubMed: 23432378]
13. Herrero MA, Lacerda L, Bianco A, Kostarelos K, Prato M. Functionalised Carbon Nanotubes: High Biocompatibility with Lack of Toxicity. Int J Nanotechnol. 2011; 8:885–897.
14. Khripin CY, Tu XM, Heddleston JM, Silvera-Batista C, Walker ARH, Fagan J, Zheng M. High-Resolution Length Fractionation of Surfactant-Dispersed Carbon Nanotubes. Anal Chem. 2013; 85:1382–1388. [PubMed: 23259532]
15. Tu XM, Walker ARH, Khripin CY, Zheng M. Evolution of DNA Sequences toward Recognition of Metallic Armchair Carbon Nanotubes. J Am Chem Soc. 2011; 133:12998–13001. [PubMed: 21777006]
16. Roxbury D, Mittal J, Jagota A. Molecular-Basis of Single- Walled Carbon Nanotube Recognition by Single-Stranded DNA. Nano Lett. 2012; 12:1464–1469. [PubMed: 22375694]
17. Roxbury D, Jagota A, Mittal J. Sequence-Specific Self- Stitching Motif of Short Single-Stranded DNA on a Single-Walled Carbon Nanotube. J Am Chem Soc. 2011; 133:13545–13550. [PubMed: 21797248]
18. Roxbury D, Tu XM, Zheng M, Jagota A. Recognition Ability of DNA for Carbon Nanotubes Correlates with Their Binding Affinity. Langmuir. 2011; 27:8282–8293. [PubMed: 21650196]
19. Shankar A, Mittal J, Jagota A. Binding between DNA and Carbon Nanotubes Strongly Depends Upon Sequence and Chirality. Langmuir. 2014; 30:3176–3183. [PubMed: 24568667]
20. Spitalsky Z, Tasis D, Papagelis K, Galiotis C. Carbon Nanotube-Polymer Composites: Chemistry, Processing, Mechanical and Electrical Properties. Prog Polym Sci. 2010; 35:357–401.
21. Sayes CM, Liang F, Hudson JL, Mendez J, Guo W, Beach JM, Moore VC, Doyle CD, West JL, Billups WE, et al. Functionalization Density Dependence of Single-Walled Carbon Nanotubes Cytotoxicity In Vitro. Toxicol Lett. 2006; 161:135–142. [PubMed: 16229976]
22. Zhang JQ, Boghossian AA, Barone PW, Rwei A, Kim J, Lin D, Heller DA, Hilmer AJ, Nair N, Reuel NF, et al. Single Molecule Detection of Nitric Oxide Enabled by D(at)(15) DNA Adsorbed to near Infrared Fluorescent Single-Walled Carbon Nanotubes. J Am Chem Soc. 2011; 133:567–581. [PubMed: 21142158]
23. Tummala NR, Morrow BH, Resasco DE, Striolo A. Stabilization of Aqueous Carbon Nanotube Dispersions Using Surfactants: Insights from Molecular Dynamics Simulations. ACS Nano. 2010; 4:7193–7204. [PubMed: 21128672]

24. Kato Y, Inoue A, Niidome Y, Nakashima N. Thermodynamics on Soluble Carbon Nanotubes: How Do DNA Molecules Replace Surfactants on Carbon Nanotubes? Sci Rep UK. 2012; 2
25. Uddin NM, Capaldi FM, Farouk B. Molecular Dynamics Simulations of Carbon Nanotube Dispersions in Water: Effects of Nanotube Length, Diameter, Chirality and Surfactant Structures. Comput Mater Sci. 2012; 53:133–144.
26. Duque JG, Oudjedi L, Crochet JJ, Tretiak S, Lounis B, Doorn SK, Cognet L. Mechanism of Electrolyte-Induced Brightening in Single-Wall Carbon Nanotubes. J Am Chem Soc. 2013; 135:3379–3382. [PubMed: 23421604]
27. Huang X, McLean RS, Zheng M. High-Resolution Length Sorting and Purification of DNA-Wrapped Carbon Nanotubes by Size- Exclusion Chromatography. Anal Chem. 2005; 77:6225–6228. [PubMed: 16194082]
28. Zheng M, Jagota A, Strano MS, Santos AP, Barone P, Chou GS, Diner BA, Dresselhaus MS, Mclean RS, Onoa GB, et al. Structure-Based Carbon Nanotube Sorting by Sequence- Dependent DNA Assembly. Science. 2003; 302:1545–1548. [PubMed: 14645843]
29. Lustig SR, Jagota A, Khripin C, Zheng M. Theory of Structure-Based Carbon Nanotube Separations by Ion-Exchange Chromatography of DNA/CNT Hybrids. J Phys Chem B. 2005; 109:2559–2566. [PubMed: 16851257]
30. Maune HT, Han SP, Barish RD, Bockrath M, Goddard WA, Rothemund PWK, Winfree E. Self-Assembly of Carbon Nanotubes into Two-Dimensional Geometries Using DNA Origami Templates. Nat Nanotechnol. 2010; 5:61–66. [PubMed: 19898497]
31. McLean RS, Huang XY, Khripin C, Jagota A, Zheng M. Controlled Two-Dimensional Pattern of Spontaneously Aligned Carbon Nanotubes. Nano Lett. 2006; 6:55–60. [PubMed: 16402787]
32. Manohar S, Tang T, Jagota A. Structure of Homopolymer DNA-CNT Hybrids. J Phys Chem C. 2007; 111:17835–17845.
33. Weisman RB, Bachilo SM. Dependence of Optical Transition Energies on Structure for Single-Walled Carbon Nanotubes in Aqueous Suspension: An Empirical Kataura Plot. Nano Lett. 2003; 3:1235–1238.
34. Tang XW, Bansaruntip S, Nakayama N, Yenilmez E, Chang YL, Wang Q. Carbon Nanotube DNA Sensor and Sensing Mechanism. Nano Lett. 2006; 6:1632–1636. [PubMed: 16895348]
35. Kim JH, Heller DA, Jin H, Barone PW, Song C, Zhang J, Trudel LJ, Wogan GN, Tannenbaum SR, Strano MS. The Rational Design of Nitric Oxide Selectivity in Single-Walled Carbon Nanotube Near-Infrared Fluorescence Sensors for Biological Detection. Nat Chem. 2009; 1:473–481. [PubMed: 21378915]
36. Staii C, Johnson AT. DNA-Decorated Carbon Nanotubes for Chemical Sensing. Nano Lett. 2005; 5:1774–1778. [PubMed: 16159222]
37. Heller DA, Baik S, Eurell TE, Strano MS. Single-Walled Carbon Nanotube Spectroscopy in Live Cells: Towards Long-Term Labels and Optical Sensors. Adv Mater (Weinheim, Ger). 2005; 17:2793–2799.
38. Barone PW, Baik S, Heller DA, Strano MS. Near- Infrared Optical Sensors Based on Single-Walled Carbon Nanotubes. Nat Mater. 2005; 4:86–92. [PubMed: 15592477]
39. Heller DA, Jin H, Martinez BM, Patel D, Miller BM, Yeung T, Jena PV, Hobartner C, Ha T, Silverman S, et al. Multimodal Optical Sensing and Analyte Specificity Using Single-Walled Carbon Nanotubes. Nat Nanotechnol. 2009; 4:114–120. [PubMed: 19197314]
40. Yang RH, Tang ZW, Yan JL, Kang HZ, Kim YM, Zhu Z, Tan WH. Noncovalent Assembly of Carbon Nanotubes and Single-Stranded DNA: An Effective Sensing Platform for Probing Biomolecular Interactions. Anal Chem. 2008; 80:7408–7413. [PubMed: 18771233]
41. Humphrey W, Dalke A, Schulten K. Vmd: Visual Molecular Dynamics. J Mol Graph Model. 1996; 14:33–38.
42. Lu XJ, Olson WK. 3DNA: A Software Package for the Analysis, Rebuilding and Visualization of Three-Dimensional Nucleic Acid Structures. Nucleic Acids Res. 2003; 31:5108–5121. [PubMed: 12930962]
43. Phillips JC, Braun R, Wang W, Gumbart J, Tajkhorshid E, Villa E, Chipot C, Skeel RD, Kale L, Schulten K. Scalable Molecular Dynamics with NAMD. J Comput Chem. 2005; 26:1781–1802. [PubMed: 16222654]

44. MacKerell AD, Bashford D, Bellot M, Dunbrack RL, Evanseck JD, Field MJ, Fischer S, Gao J, Guo H, Ha S, et al. All-Atom Empirical Potential for Molecular Modeling and Dynamics Studies of Proteins. J Phys Chem B. 1998; 102:3586–3616. [PubMed: 24889800]
45. Hornak V, Abel R, Okur A, Strockbine B, Roitberg A, Simmerling C. Comparison of Multiple Amber Force Fields and Development of Improved Protein Backbone Parameters. Proteins. 2006; 65:712–725. [PubMed: 16981200]
46. Perez A, Marchan I, Svozil D, Sponer J, Cheatham TE 3rd, Laughton CA, Orozco M. Refinement of the Amber Force Field for Nucleic Acids: Improving the Description of Alpha/Gamma Conformers. Biophys J. 2007; 92:3817–3829. [PubMed: 17351000]
47. Darden T, York D, Pedersen L. Particle Mesh Ewald - an N.Log(N) Method for Ewald Sums in Large Systems. J Chem Phys. 1993; 98:10089–10092.
48. Cathcart H, Nicolosi V, Hughes JM, Blau WJ, Kelly JM, Quinn SJ, Coleman JN. Ordered DNA Wrapping Switches on Luminescence in Single-Walled Nanotube Dispersions. J Am Chem Soc. 2008; 130:12734–44. [PubMed: 18761456]
49. Moore VC, Strano MS, Haroz EH, Hauge RH, Smalley RE, Schmidt J, Talmon Y. Individually Suspended Single- Walled Carbon Nanotubes in Various Surfactants. Nano Lett. 2003; 3:1379–1382.
50. Bachilo SM, Strano MS, Kittrell C, Hauge RH, Smalley RE, Weisman RB. Structure-Assigned Optical Spectra of Single- Walled Carbon Nanotubes. Science. 2002; 298:2361–2366. [PubMed: 12459549]
51. Dukovic G, Balaz M, Doak P, Berova ND, Zheng M, McLean RS, Brus LE. Racemic Single-Walled Carbon Nanotubes Exhibit Circular Dichroism when Wrapped with DNA. J Am Chem Soc. 2006; 128:9004–5. [PubMed: 16834352]
52. Burge S, Parkinson GN, Hazel P, Todd AK, Neidle S. Quadruplex DNA: Sequence, Topology and Structure. Nucleic Acids Res. 2006; 34:5402–5415. [PubMed: 17012276]
53. Johnson RR, Johnson ATC, Klein ML. Probing the Structure of DNA-Carbon Nanotube Hybrids with Molecular Dynamics. Nano Lett. 2008; 8:69–75. [PubMed: 18069867]
54. Johnson RR, Johnson ATC, Klein ML. The Nature of DNA-Base-Carbon-Nanotube Interactions. Small. 2010; 6:31–34. [PubMed: 19943252]
55. Johnson RR, Kohlmeyer A, Johnson ATC, Klein ML. Free Energy Landscape of a DNA-Carbon Nanotube Hybrid Using Replica Exchange Molecular Dynamics. Nano Lett. 2009; 9:537–541. [PubMed: 19161335]
56. Karachevtsev MV, Gladchenko GO, Plokhotnichenko AM, Leontiev VS, Karachevtsev VA. Adsorption of Biopolymers on Swcnt: Ordered Poly(Rc) and Disordered Poly(Ri). J Phys Chem B. 2013; 117:2636–2644. [PubMed: 23402540]
57. Lee AJ, Wang XY, Carlson LJ, Smyder JA, Loesch B, Tu XM, Zheng M, Krauss TD. Bright Fluorescence from Individual Single-Walled Carbon Nanotubes. Nano Lett. 2011; 11:1636–1640. [PubMed: 21417364]

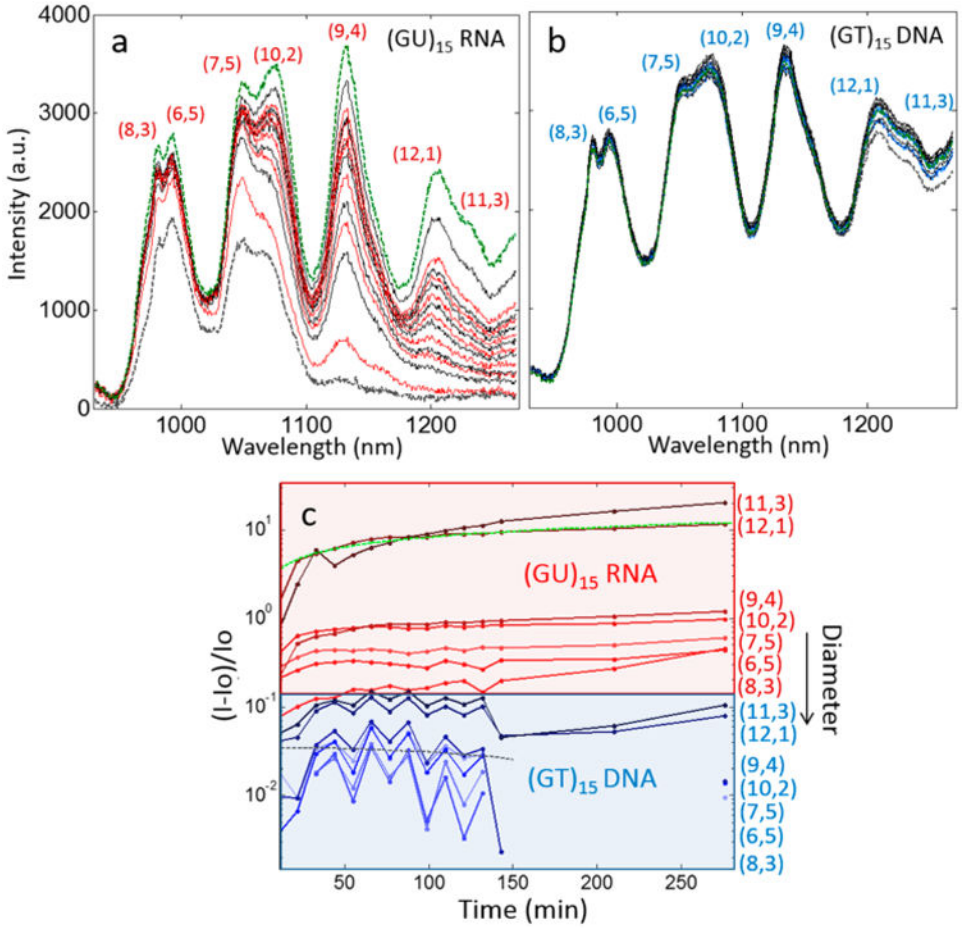

Figure 1.

DNA and RNA polymer conformational stability is monitored with increasing SWCNT fluorescence. Fluorescence emission spectra of 1 mg/L (a) $(GU)_{15}$ RNA-SWCNT and (b) $(GT)_{15}$ DNA-SWCNT over the course of 275 min, with 785 nm, 200 mW excitation source, and 10 s exposure time. Each peak corresponds to the emission of a particular SWCNT chirality from a multichirality SWCNT sample, where the first and last spectra are highlighted as dashed gray and dashed green, respectively. (c) Emission peak for each SWCNT chirality normalized to the initial intensity for $(GT)_{15}$ DNA-SWCNT (blue) and $(GU)_{15}$ RNA-SWCNT (red) over the same time-course. The data for the (7,6) SWCNT chirality for $(GU)_{15}$ RNA-SWCNT (green dashed line) and $(GT)_{15}$ DNA-SWCNT (gray dashed line) is fit by a kinetic model described in the manuscript text. Each plotted line is labeled by the corresponding SWCNT chirality. SWCNT diameter decreases from top to bottom of each of the DNA (blue) and RNA (red) regions of the graph.

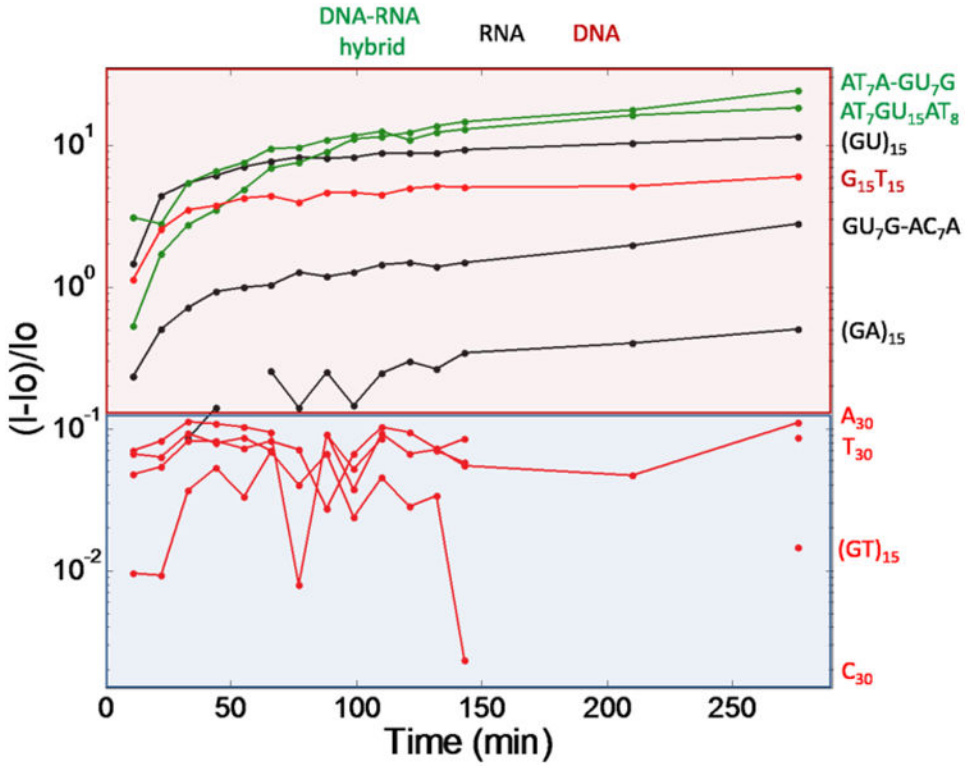

Figure 2.

Analysis of DNA, RNA, and DNA–RNA polymer hybrids for conformational stability on SWCNT. Emission peak for (9,4) chirality SWCNT at 1133 nm, normalized to the initial sample intensity for ten different polynucleotide corona phases comprised of DNA (red), RNA (black), or DNA–RNA hybrid (green) sequence variants. Nucleotide polymer stability is similarly high across DNA sequences (blue shaded region) and lower for RNA or DNA–RNA hybrid sequences (red shaded region). A notable exception is $G_{15}T_{15}$ DNA, which is known to form secondary G-quadruplex structures,[52] and is expected to form such secondary structures off the SWCNT surface.

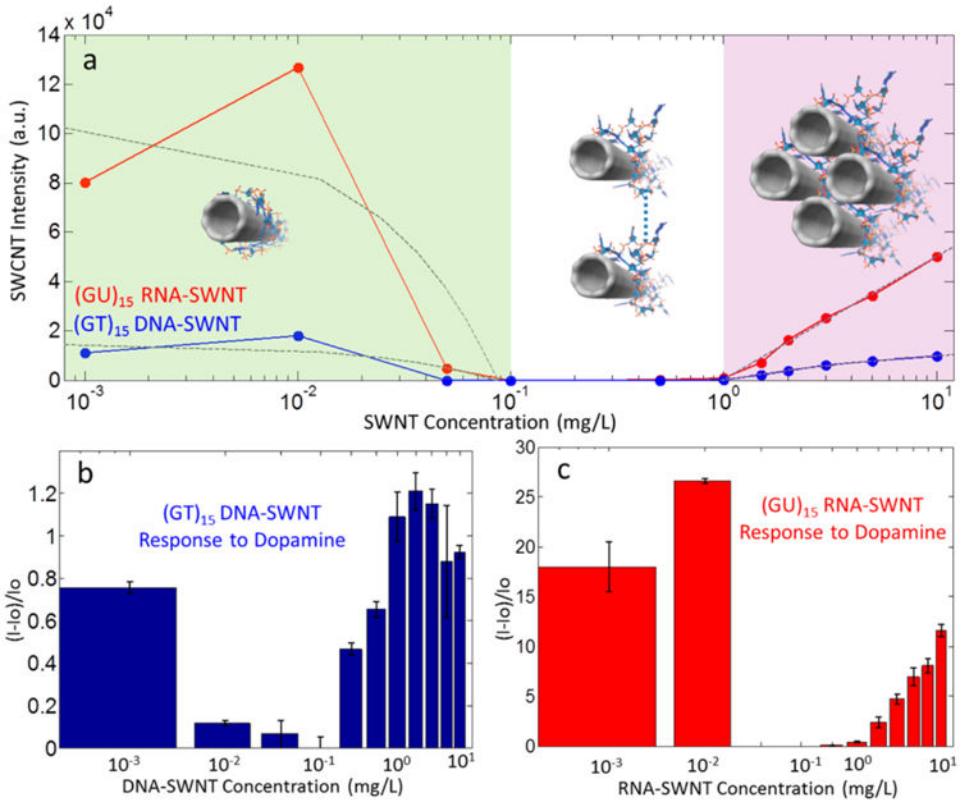

Figure 3.

Experimental concentration-dependent fluorescence intensity of DNA and RNA-SWCNT samples, and sensor response. (a) Intensity of $(GT)_{15}$ DNA-SWCNT (blue) and $(GU)_{15}$ RNA-SWCNT (red) as a function of SWCNT concentration from 10^{-3} to 101 mg/L. In the low- concentration regime (below 10^{-1} mg/L, green shaded region), SWCNT fluorescence is dominated by high-intensity emitters resulting from strong stacking of DNA or RNA nucleotides on the SWCNT surface. In the high-concentration regime (above 100 mg/L SWCNT, purple shaded region), SWCNT fluorescence is dominated by large quantities of low-intensity polynucleotide-SWCNT complexes. The intermediate concentration range (10^{-1} to 100 mg/L SWCNT, unshaded region) shows primarily loose-nucleotide stacking species for which the concentration is too low to detect SWCNT emitters. (b) The fluorescence response, (I – Io)/Io, to 100 μM dopamine for these same dilutions of $(GT)_{15}$ DNA-SWCNT and (c) $(GU)_{15}$ RNA-SWCNT at 1130 nm.

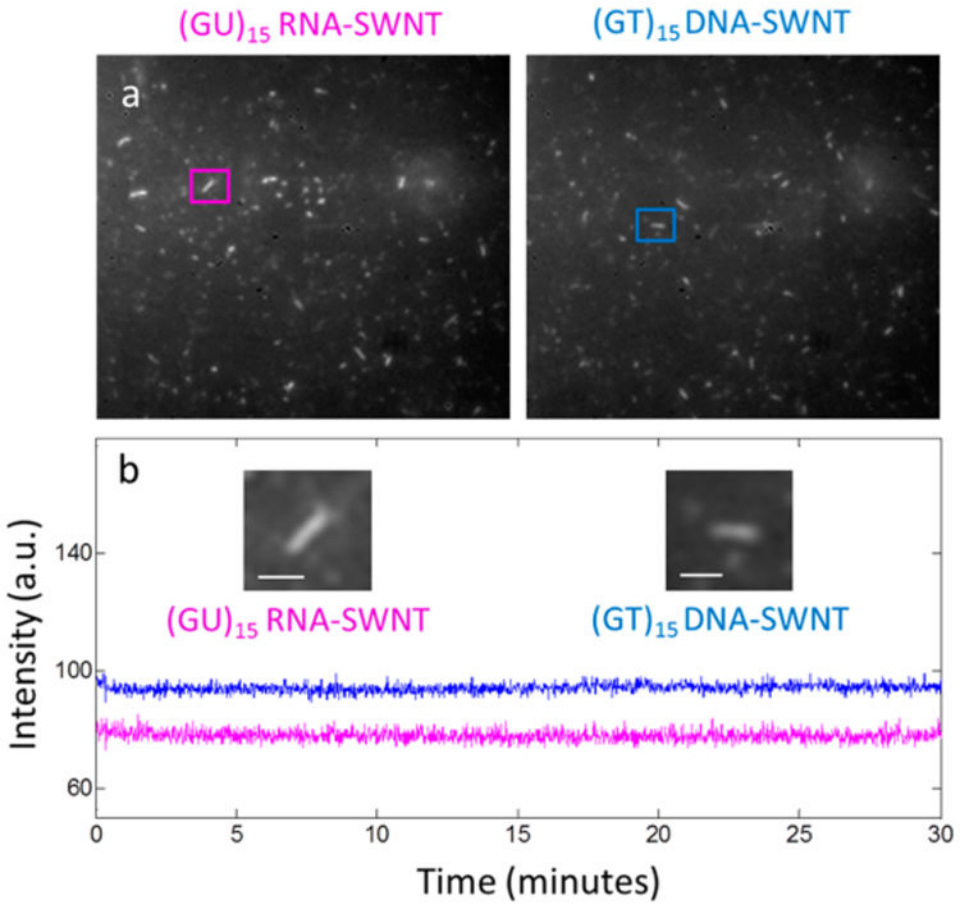

Figure 4.

Single-SWCNT imaging of $(GU)_{15}$ RNA-SWCNT and $(GT)_{15}$ DNA-SWCNT fluorescence stability. (a) Surface-immobilized $(GU)_{15}$ RNA-SWCNT and $(GT)_{15}$ DNA-SWCNT within a micro-fluidic channel can be individually monitored for 30 min. (b) Representative individual $(GU)_{15}$ RNA-SWCNT (purple) and $(GT)_{15}$ DNA-SWCNT (blue) intensities over the course of 30 min, at 785 nm 200 mW excitation, and 1 s exposure time. Scale = 1 μm.

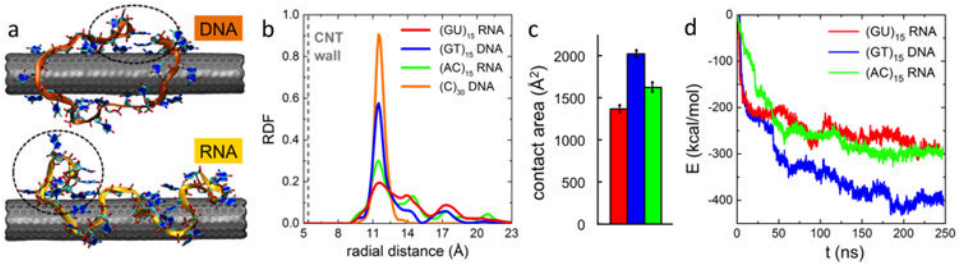

Figure 5.

Molecular dynamics of DNA and RNA binding to SWCNT. (a) Snapshots of SWCNT and single $(GT)_{15}$DNA and $(GU)_{15}$RNA strands at the end of 250 ns MD simulations. SWCNT is shown in charcoal, nucleic acid strands are shown in licorice representations, and polynucleotide phosphate backbones are highlighted in orange or gold. Water and ions are not shown for clarity, though have an increased proximity to SWCNT when nucleotides desorb from the SWCNT surface. Nucleic acid atoms are shown in teal (C), red (O), tan (P), and blue (N) colors. (b) Radial distribution of phosphate groups (P atoms) of nucleic acid strands at distance r from the central axis of SWCNT, evaluated for the last 100 ns of simulations. (c) Contact areas between SWCNT and nucleic acid strands, averaged over the last 100 ns of simulations. (d) Interaction energies between SWCNT and nucleic acid strands (including van der Waals contributions; Coulombic contributions are null due to SWCNT atoms having no partial charges, $q_{CA} = 0$ e). The plots shown in (b–d) are representative of the subset of possible nucleic acid configurations, captured in the performed MD simulations.

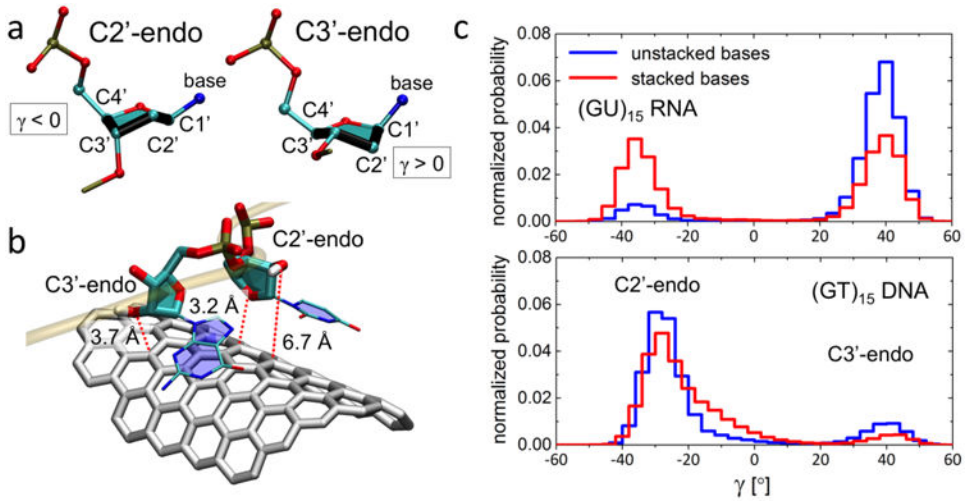

Figure 6.

Sugar conformations in nucleic acid strands interacting with SWCNTs. (a) A scheme of C2′-endo and C3′-endo sugar conformations, commonly observed in B-form DNA and A-form DNA/RNA, respectively. The sugar conformation can be characterized by the dihedral angle γ (C4′–C3′–C2′–C1′), which is highlighted in black bond representation; $\gamma < 0°$ in the C2′-endo conformation, and $\gamma > 0°$ in the C3′-endo conformation. (b) A representative simulation snapshot of RNA backbone and sugar rings when RNA bases are stacking to the SWCNT. 2′-OH group of the RNA nucleotide can point toward the SWCNT surface (C3′-endo conformation of the sugar ring) or away from the SWCNT surface (C2′-endo conformation; O4′ oxygen points to the SWCNT surface). In (a, b), SWCNT atoms are shown in light gray, and nucleic acid atoms are shown in teal (C), red (O), tan (P), blue (N), and white (H) colors. The transparent yellow line shows RNA backbone in tube representation. (c) Histogram distributions of the angle γ, shown separately for bases that are stacked on SWCNT and bases that are not stacked on SWCNT. Histogram distributions are obtained from complete (250 ns) simulations of $(GT)_{15}$ DNA-SWCNT and $(GU)_{15}$ RNA-SWCNT systems.